JOURNAL OF GEOPHYSICAL RESEARCH, VOL. 106, NO. C10, PAGES 22,339–22,353, OCTOBER 15, 2001

A quasi-one-dimensional coupled climate–change cycle model 1. Description and behavior of the climate component

L. D. Danny Harvey and Z. Huang[1]

Department of Geography, University of Toronto, Toronto, Ontario, Canada

Abstract. A quasi-one-dimensional, coupled climate – carbon cycle model is presented, which consists of two polar domains and one nonpolar domain. The model simulates the distribution of dissolved inorganic carbon (DIC), alkalinity, phosphate, dissolved oxygen, and temperature and contains a biological pump with production of organic tissue, calcite, and arogonite. Bottom water is conditioned in one polar domain through interaction with the atmosphere and convective mixing and is injected into the lower portion of the nonpolar domain. Bottom water formed in the downwelling polar domain largely upwells in the nonpolar domain, although a portion upwells from intermediate depth into the other polar domain. In this paper the climate component of the coupled model and its behavior are described, while the carbon cycle component is documented by *Harvey* [this issue], hereafter referred to as part 2. We develop a simple physical basis for determining the relative magnitudes of the effective vertical diffusion coefficient (k_v) for different tracers in a one – dimensional (1-D) model and find that k_v is smallest for temperature, intermediate for carbon, and largest for dissolved oxygen. We deduce a substantially smaller k_v for temperature in the upper ocean than previously used in 1-D models (~0.2 $cm^2 s^{-2}$ rather than 0.6-1.0 $cm^2 s^{-1}$) and a smaller peak upwelling velocity (2 m yr^{-1} rather than 4 m yr^{-1}). The explicit representation of convective mixing has a significant effect on the model surface temperature transient response and sea level rise when the intensity of the thermohaline changes. As a result, the transient temperature response and sea level rise obtained here when the thermohaline circulation intensity decreases is significantly different from that of the classical 1-D upwelling-diffusion model.

1. Introduction

One–dimensional (1-D) vertically resolved ocean models combined with a one-box atmospheric model have been extensively used to study the transient surface temperature response to external forcing changes [e.g., *Hoffert et al.*, 1980; *Harvey and Schneider*, 1985; *Watts*, 1985; *Gaffen et al.*, 1986; *Wigley and Raper*, 1990a; *Schlesinger and Ramankutty*, 1992; *Kelly and Wigley*, 1992; *Kattenburg et al.*, 1996; *Wigley et al.*, 1997; *Joos et al.*, 1999; *Harvey*, this issue] in computing past and future sea level rise due to thermal expansion of the oceans [*Wigley and Raper*, 1987, 1990b], and in computing the oceanic uptake of anthropogenic CO_2 [*Oeschger et al.*, 1975; *Hoffert et al.*, 1981; *Siegenthaler*, 1983; *Siegenthaler and Joos*, 1992; *Joos et al.*, 1999]. In most of these papers the 1-D upwelling diffusion (UD) model or a variant of it has been used. The upwelling diffusion model has also been fitted to the transient response of coupled atmosphere-ocean general circulation models (AOGCMs) in order to estimate the corresponding AOGCM climate sensitivity [*Raper and Cubasch*, 1996]. *Harvey et al.* [1997] review the role of simple and complex models in assessing the impacts on climate of alternative greenhouse gas and aerosol-precursor emission scenarios.

An important parameter in the oceanic uptake of heat and CO_2 is the value of the vertical diffusion coefficient (K_v). This parameter must be externally prescribed in both 1-D and three–dimensional (3-D) ocean models, with the prescribed value of K_v strongly influencing the results of 1-D models and the dynamics of 3-D models [*Bryan*, 1987]. The K_v in 1-D models is an effective global mean value representing a number of mixing processes (such as convection) that are not explicitly represented in most 1-D models. Considerable effort has been devoted in the past to estimating the appropriate value of the vertical diffusion coefficient for use in 1-D models by tuning these models to fit various observations. Values obtained by tuning a model to replicate the preindustrial distribution of $\Delta^{14}C$ tend to be smaller (e.g., 0.49 $cm^2 s^{-1}$ according to *Shaffer and Sarmiento* [1995]; 0.70 $cm^2 s^{-1}$ according to *Siegenthaler* [1983]; 1.26 $cm^2 s^{-1}$ according to Oeschger et al. [1975] than values obtained by tuning a model to replicate the observed uptake of bomb ^{14}C (e.g., 1.64 $cm^2 s^{-1}$ according to *Siegenthaler* [1983]. *Siegenthaler and Joos* [1992] found that they could simultaneously replicate the observed preindustrial ^{14}C distribution and uptake of bomb ^{14}C only if they assumed that K_v varied with depth, with best results when K_v decreased from 2.4 $cm^2 s^{-1}$ at the surface to 0.14 $cm^2 s^{-1}$ in the deep ocean. For the case in which K_v is assumed to be constant with depth, *Siegenthaler and Joos* [1992] also found that the K_v required to simulate the observed vertical variation in global mean ocean temperature (namely, 0.27 $cm^2 s^{-1}$) is smaller than that required in order to fit either the bomb or preindustrial ^{14}C distributions. *Hoffert et al.* [1981] obtained a larger K_v (0.63 $cm^2 s^{-1}$) based on the temperature profile, but the required K_v will scale up or down in direct propor-

[1]Currently at Atmospheric and Climate Sciences Group, Earth and Environment Sciences Division, Los Alamos National Laboratory, Los Alamos, New Mexico.

Paper number 2000JC000364.
0148-0227/01/2000JC000364$09.00

tion to the assumed upwelling velocity (which both *Siegenthaler and Joos* [1992] and *Hoffert et al.* [1981] took to be constant with depth).

In spite of the uncertainty and disagreement concerning the appropriate value of K_v, there has been no systematic investigation of the impact of changes in the prescribed value of K_v (or of the upwelling velocity) on future atmospheric CO_2 concentrations. *Jain et al.* [1995, 1996] show that the model of *Hoffert et al.* [1981], with close to the original parameter values, can closely replicate the observed preindustrial oceanic profiles and transient variations of ^{13}C and ^{14}C in the atmosphere, but they did not show the effect of parameter changes on the model performance nor on future atmospheric CO_2 concentrations. Thus it is not known if alternative parameter combinations could give comparable fits to observations and what effect these alternatives would have on future projections.

The purpose of this paper and *Harvey* [this issue], hereafter referred to as part 2, is to present a relatively simple coupled atmosphere-ocean climate-carbon cycle model that can be used to simulate the concurrent uptake of both heat and CO_2 by the oceans and associated changes in sea level due to ocean thermal expansion. The major motivations in this work are to develop a model which can be used to examine the interaction of a number of possible climate, ocean circulation, and carbon cycle feedback processes; to develop a model which can be easily used for analysis of alternative scenarios concerning anthropogenic greenhouse gas and aerosol emissions; and to develop a model which can be used to investigate natural climate and carbon cycle fluctuations at geological timescales. The model to be presented here is not intended to predict changes in oceanic circulation. Rather, the present model is intended as a tool to diagnose the appropriate present-day mixing parameters (within observational constraints) and in analyzing the effect on the uptake of both heat and CO_2 of imposed feedbacks between climate and oceanic mixing.

The focus of interest here is on global-scale changes. For these reasons, we have developed a model consisting of three horizontal domains, with vertical resolution in each oceanic domain and a vertically well-mixed atmosphere. In this paper we present the model structure and our formulation of ocean mixing processes and then demonstrate that the transient surface temperature response and sea level rise predicted by the climate

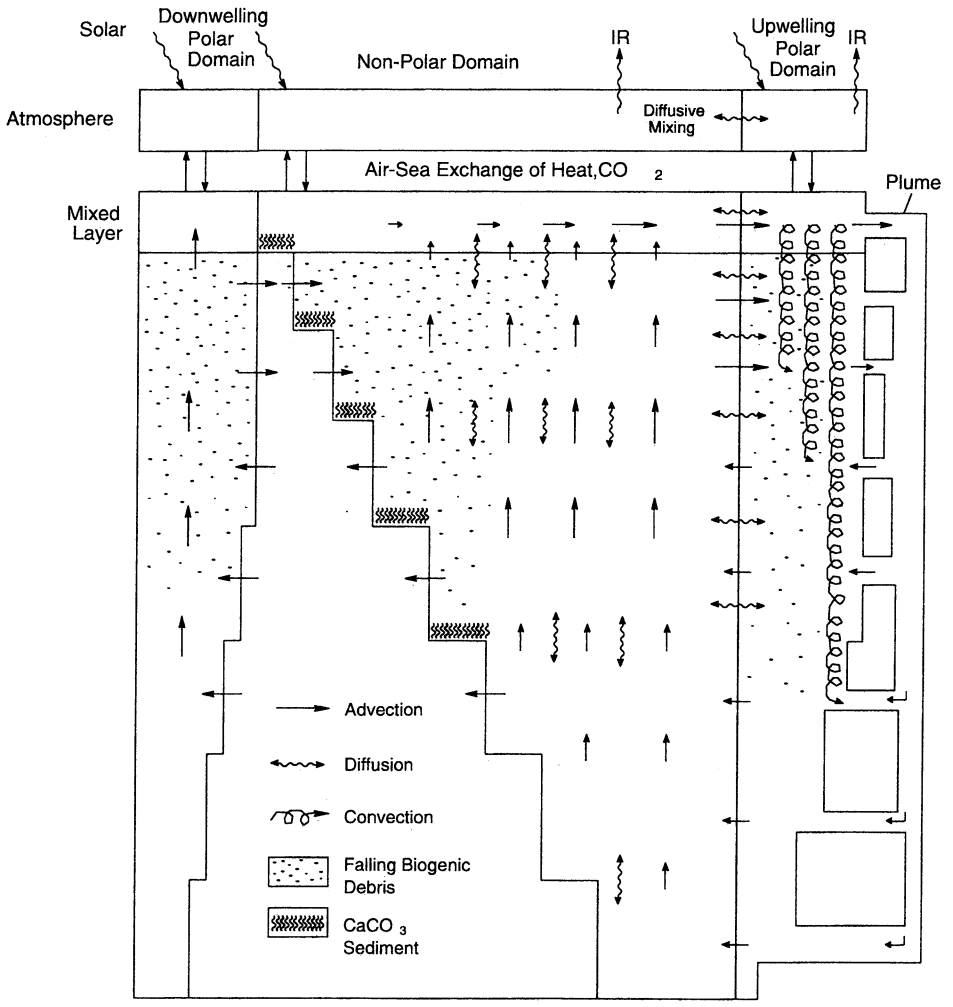

Figure 1. Schematic illustration of the model, showing the polar and nonpolar domains and vertical fluxes due to thermohaline overturning (advection), diffusion, convection, and falling biogenic material. The subsurface Southern Hemisphere (SH) polar domain is drawn with a gap between it and the nonpolar domain only for convenience.

component of this model is distinctly different from that of the widely used upwelling-diffusion model for a number of perturbations of interest. In part 2, *Harvey* [this issue] provides details on the formulation and behavior of the carbon cycle component of the model. In particular, it is shown that the model does very well in simulating observed steady state tracer profiles in the ocean and transient atmospheric isotope variations.

2. Model Description

2.1. Overview and Major Differences From Previous One–Dimensional Models

The model presented here contains atmospheric, oceanic, and terrestrial biosphere components. The atmospheric component of the model, including the formulation of surface-air exchanges of sensible and latent heat, infrared radiation, and solar radiation, is that of *Harvey and Schneider* [1985]. The atmospheric and oceanic components are illustrated schematically in Figure 1. Both the atmosphere and the ocean have two polar domains and a nonpolar domain. In addition to the domains shown in Figure 1, a combined atmosphere-land surface (ALS) slab interacts directly with the atmosphere of the nonpolar domain. The ALS slab has a heat capacity equal to that of the atmosphere plus a 1.7 m thick layer of water, is driven by the global mean incident solar radiation, and has an area fraction of 0.3 the global surface area. The sole purpose of the ASL slab is to allow for the effect of the low thermal inertia over land in the transient global mean atmospheric temperature response. In *Harvey and Schneider* [1985] the effect of the small land thermal inertia was accounted for by reducing the thickness of the oceanic mixed layer, but here we need to use the real physical mixed layer depth because the mixed layer here is also part of the model carbon cycle.

Previous work has demonstrated the importance to the carbon cycle of the direct coupling of the atmosphere to the deep ocean through polar regions of convective mixing and bottom water formation [e.g., *Siegenthaler*, 1983]. In nature, bottom water forms primarily in the North Atlantic Ocean and in the Weddell Sea region. However, there is also significant upwelling of Atlantic Intermediate Water in the circum-Antarctic region, a process that could modulate the downward penetration of anthropogenic CO_2 due to convective mixing in this region. We therefore distinguish two polar domains in the model. The first, referred to as the downwelling polar domain (DPD), represents all those polar regions, in both hemispheres, where bottom water forms. The second polar domain represents the Southern Hemisphere regions where upwelling of intermediate-depth water occurs and is referred to as the upwelling polar domain (UPD). Within both polar domains of the ocean, a distribution of convective mixing depths is assumed. Water flows horizontally from the nonpolar domain into the downwelling polar domain in the upper part of the ocean, is conditioned by interaction with the atmosphere and through convective mixing with deeper water, and then enters a polar boundary layer plume (represented by the tube to the right in Figure 1) which sinks to the bottom of the ocean. We allow for a separate plume adjacent to the downwelling polar domain because much of the bottom water which forms in nature sinks as a plume along sloping continental shelves in polar regions (see the review by *Harvey* [1996]). The downwelling polar column represents the source regions where water is conditioned before entering the plume. As in nature, entrainment of water into the sinking plume occurs in the upper ocean, while gradual detrainment occurs in the deeper ocean. The water that detrains is assumed to spread laterally and upwell largely in the nonpolar domain, where the primary balance is between vertical diffusion and upwelling. Some of the upwelling water enters the upwelling polar domain, primarily above the 4000 m depth, and re-enters the nonpolar domain within the upper kilometer of the ocean. Weak lateral diffusive mixing between the polar and nonpolar domains also occurs. We allow the area of the nonpolar domain to vary with depth, based on observed bathymetry.

Polar downwelling and upwelling regions need to be distinguished so that reasonable polar and nonpolar values for the coefficient for air-sea gas exchange can be used while still fitting ^{14}C observations. The fact that Southern Hemisphere upwelling and downwelling regions are placed in two separate domains is not critical except to the extent that direct mixing between the two occurs in nature but not in the model. Indeed, there appears to be considerable recirculation between upwelling and downwelling regions in the Southern Hemisphere in nature, based on the 3-D model simulation results of *Döös and Webb* [1994]. However, the polar upwelling flux used here (~5 Sv) represents only net flow from abyssal nonpolar regions to the Southern Hemisphere polar region. That is, it represents "aged" (^{14}C-depleted) water and can be treated separately from Southern Hemisphere downwelling water, which in turn can be lumped with Northern Hemisphere downwelling water.

As discussed in part 2, biological activity in the mixed layer of each domain produces a rain of organic carbon and calcium carbonate. A portion of the biogenic debris landing on the ocean bottom is assumed to be oxidized or to dissolve, while the rest undergoes permanent burial. The tracers whose distribution is simulated are all three isotopes of dissolved inorganic carbon (DIC, the sum of dissolved CO_2, CO_3^{2-}, and HCO_3^-), total alkalinity (TALK), dissolved oxygen, total dissolved phosphate (PO_4), and temperature. The burial fluxes of carbon, alkalinity, and PO_4 are balanced by riverine and volcanic (in the case of carbon) fluxes to the mixed layer (or atmosphere).

Previously developed 1-D ocean carbon cycle models were built around one of three structures: the pure-diffusion model of *Oeschger et al.* [1975], of which the outcrop-diffusion model of *Siegenthaler* [1983] is a variant; the UD model of *Hoffert et al.* [1980, 1981], which assumes the existence of a polar sea where bottom water forms but does not explicitly resolve the polar sea; and the UD model with a single explicitly resolved polar sea surface layer, either with [*Siegenthaler and Joos*, 1992] or without [*Kheshgi et al.*, 1991] an infinitely mixed subsurface polar box.

The present model is similar to that of *Siegenthaler and Joos* [1992], which has been dubbed the "HILDA" model, except that it has two rather than one polar column and the polar columns are not assumed to be infinitely mixed below the mixed layer. *Siegenthaler and Joos* [1992] allow K_v to vary with depth, as we do, but the shape of the variation adopted by *Siegenthaler and Joos* [1992] is substantially different from that adopted here. Other workers have not allowed the vertical velocity w to vary with depth and, with the exception of *Kheshgi et al.* [1991], do not allow the ocean area to vary with depth. As discussed in part 2, finite mixing in the polar sea, the use of observed bathymetry, and depth-dependent K_v and w are all critical to the successful simultaneous simulation of all the model ocean tracers. In the *Hoffert et al.* [1981] model the temperature and DIC of sinking polar water are prescribed, whereas here and in the HILDA model they are freely predicted. The Hoffert model

contains a biological pump of fixed strength, and all biogenic debris settles on an ocean bottom at the same depth (4000 m), whereas here the biological pump strength depends on the model-predicted concentration of phosphate in the mixed layer, and biogenic debris dissolves over a range of ocean depths. The original HILDA model did not contain the biological pump. *Shaffer* [1996] presented an extension of the original HILDA which contains the organic tissue pump but, unlike the model presented here, did not include the production of $CaCO_3$. Thus the model presented here and in part 2 differs in several important ways from previous simple ocean models.

The present model also differs from previous 1-D models in that more variables are simultaneously simulated, thereby providing greater observational constraints for tuning the model parameters and providing for a greater range of feedback interactions. For example, a change in the thermohaline overturning intensity (represented by the upwelling velocity) affects the mixed layer DIC through its effect in the vertical flux of DIC, on the biological pump strength (which depends on the upwelling of phosphate), and through changes in the surface alkalinity (which alters the pCO_2 for a given DIC, leading to exchanges of CO_2 between the atmosphere and mixed layer). With the exception of *Khesghi et al.* [1991], previous 1-D models either do not simulate the alkalinity field [e.g., *Siegenthaler and Joos*, 1992], assume a fixed biological productivity [e.g., *Hoffert et al.*, 1981], or neglect the marine biota altogether [e.g., *Oeschger et al.*, 1975].

In summary, the major novel features of the present model are (1) the model structure, (2) the formulation of the upwelling velocity and vertical diffusion coefficient, (3) the formulation of finite convective mixing in the polar columns, (4) the inclusion of alkalinity as a variable (usually lacking in 1-D models), and (5) the partial oxidation of buried organic carbon (giving a net burial that is smaller than gross burial). All of these features are important to the model simulation of present conditions and, in some cases, are also important to the model response to perturbations. As well, the model uses a novel solution algorithm that involves a mixture of numerical and analytical techniques, thereby permitting the use of 1-year time steps.

In the following sections 2.2-2.6 we discuss in more detail those features of the mode that are relevant to both the climate and carbon cycle components, while deferring a more detailed discussion of the purely carbon cycle features to part 2. Details concerning the governing equations and the solution algorithm are presented in appendices A and B.

2.2. Vertical Variation of Upwelling Velocity

The upwelling velocity in the nonpolar domain (and in the UPD) is prescribed as in previous UD models. This upwelling balances the downwelling in polar regions. Observations summarized by *Harvey* [1996] indicate that entrainment of water adjacent to sinking polar plumes increases the plume flux by about a factor of 3 between the source shelf areas (400-1000 m depth) and the depth at which detrainment begins. The North Atlantic plume descends to a depth of 3000-4000 m, while the Weddell Sea plume (which forms Antarctic Bottom Water) reaches even greater depths. The total flux associated with the two plumes is estimated to be ~18-26 Sv (1 Sv = 1.0 x 10^6 m^3 s^{-1}), which corresponds to an upwelling velocity w, averaged over the remaining ocean, of 1.6-2.3 m yr^{-1}. Inasmuch as some bottom water may form in nature outside of boundary layer plumes, the appropriate peak upwelling velocity could be larger. In any case, we shall adopt a nonpolar upwelling flux which peaks at some mid-ocean depth, rather than assuming it to be constant between the surface and ocean bottom (as in previous UD models). With regard to the upwelling flux in the upwelling polar column, we shall assume a peak flux of around 5 Sv, as this is roughly the portion of the total upwelling flux in the circum-Antarctic region that involves water from the NH that flows into this upwelling region in the OGCM simulation of *Döös and Webb* [1994].

2.3. Formulation of K_X and Its Vertical Variation

The vertical diffusion coefficient used in the nonpolar domain (Appendix A), K_X, is an effective coefficient that represents the net effect of mixing perpendicular to and along sloping isopycnal surfaces. The diapycnal (perpendicular) component, K_n, is parameterized as by *Gargett* [1984], namely,

$$Kn = \frac{Ao}{\left(\frac{g}{\rho}\frac{\partial \rho}{\partial z}\right)^{1/2}}, \quad (1)$$

where ρ is potential density. The physical basis of this parameterization is that diapycnal mixing (which is overwhelmingly vertical) will be easier the less stratified the ocean column is. Since salinity is not predicted by the model, the observed variation of mean salinity outside the polar domain, as given by *Levitus* [1982], is used along with the model-predicted temperature in computing the density profile.

As discussed by *Harvey* [1995], the effective vertical diffusion coefficient when mixing along sloping isopycnal surfaces is taken into account is given by

$$K_{\text{eff}} = \frac{1}{1+\delta^2}\left[K_n + \delta^2 K_i + \left(\frac{\partial X/\partial x}{\partial X/\partial z}\right)\delta(K_i - K_n)\right], \quad (2)$$

where δ is the slope of isopycnal surfaces and K_i is the isopycnal diffusivity. Given that K_i is ~7 orders of magnitude larger than K_n and that δ can reach values of 10^{-4} in the upper kilometer of the ocean at middle to high latitudes, it can be readily seen that K_{eff} can easily be an order of magnitude larger than K_n. Furthermore, $(\partial X/\partial x)/(\partial X/\partial z)$ will in general be different for different tracers, so that the corresponding K_{eff} values will differ. However, as given by *Harvey* [1995], global mean values of K_n and K_{eff} for temperature are almost the same at all depths, owing to the fact the isotherms and isopycnals are almost exactly parallel, so that there is almost no temperature gradient on isopycnal surfaces.

We attempted to compute the vertical variation of the global mean K_{eff} for other tracers based on (1) basin-averaged observed data for temperature and salinity from *Levitus* [1982], from which one can compute the density field and hence K_n and the slope terms appearing in equation (2) and (2) basin-averaged observed concentrations for the other tracers, from which one can compute the gradients appearing in equation (2). However, the *Levitus* [1982] data set contains numerous instances of unstable vertical profiles, such that the original temperatures or salinities have to be adjusted. Even after this adjustment, the global mean (flux-weighted) K_{eff} values at a given depth are often dominated by very large values at one or two horizontal grid points. As a result, there is considerable scatter in the computed vertical variation of K_{eff}, and this approach is not reliable.

We can nevertheless obtain a sense of how K_{eff} should differ between different tracers by considering representative low-

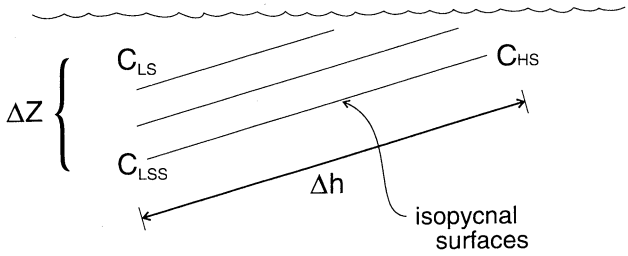

Figure 2. Schematic illustration showing the relationship between tracer concentrations at the low and high latitude surface and at the low-latitude subsurface (C_{LS}, C_{HS}, and C_{LSS}) on the one hand, and sloping isopycnal surfaces on the other hand.

latitude (30°) and high–latitude (60°) surface tracer concentrations (C_{LS} and C_{HS}, respectively) and subsurface concentrations at low latitudes (C_{LSS}). Figure 2 shows these three points in relation to those isopycnal surfaces which outcrop near 60°N; these isopycnal surfaces reach a depth of ~600-1000 m at 30°N, over a distance Δh of ~3000 km. Table 1 gives rough C_{LS}, C_{HS}, and C_{LSS} values for six tracers, averaged over all ocean basins in both hemispheres, estimated from surface maps of OGCM simulations or cross sections of GEOSECS data given in *Bacastow and Maier-Reimer* [1990]. The vertical flux F_i due to mixing along isopycnal surfaces is given by

$$F_i = -\frac{\delta}{\sqrt{1+\delta^2}} K_i \frac{\partial C}{\partial h} \approx -\frac{\delta}{\sqrt{1+\delta^2}} K_i \frac{C_{HS} - C_{LSS}}{\Delta h}, \quad (3)$$

while the vertical flux due to diapycnal mixing, F_n, is given by

$$F_n \approx -K_n \frac{\partial C}{\partial z} = -K_n \frac{C_{LS} - C_{LSS}}{\Delta z}. \quad (4)$$

Table 1 gives F_n and F_i, computed assuming that $K_n = 0.2$ cm^2 s^{-1}, $K_i = 1.0 \times 10^2$, and $\delta = 2.0 \times 10^{-4}$. The last column of Table 1 gives the ratio of K_{eff} to K_n, where K_{eff} is computed as $(F_i+F_n)/(\partial C/\partial z)$.

The ratio K_{eff}:K_n is controlled by the strength and direction of the latitudinal variation in the surface tracer concentration compared to the variation with increasing depth at low latitudes. K_{eff}:K_n is largest for O_2 because its concentration increases toward the pole in the surface layer while decreasing with increasing depth at low latitudes, the combination of which leads to a particularly strong gradient on isopycnal surfaces. Conversely, K_{eff}:K_n is smallest for PO_4 and TALK because the concentration increases toward the pole in the surface layer and with increasing depth at low latitudes, which leads to a weaker gradient on isopycnal surfaces. Thus, in spite of considerable uncertainty concerning the appropriate absolute values for K_{eff}, there is no doubt that K_{eff} should be significantly larger for O_2 than for DIC, identical for all three isotopes of DIC, and modestly smaller for TALK and PO_4.

In light of the above, we represent K_X as

$$K_X(z) = \begin{cases} K_n(z) & \text{temperature} \\ K_n(z) + K_{1x}(z) & \text{all other tracers} \end{cases}, \quad (5)$$

where $K_{1X}(z)$ is the enhancement in K_X due to isopycnal mixing for tracer X. Since $K_{1X}(z)$ arises only for the non-temperature tracers, further discussion is deferred until part 2. However, it is worth noting that K_{eff} differs most strongly between temperature and those tracers that have an important subsurface source (as in the case of PO_4) or sink (as in the case of O_2), which leads to nonnegligible gradients on isopycnal surfaces. Furthermore, PO_4 and O_2 have a K_{eff} that differ from each other because one has a subsurface source and the other a subsurface sink and because of differing surface boundary conditions.

Although we have attempted to account for the difference between diapycnal and isopycnal diffusion in our formulation of K_{eff}, we have done so on the basis of steady state tracer profiles. It could be argued that the magnitude and/or relative ranking of the K_{eff} for different tracers might change during the transition to a new climate state (for example, greater warming at high latitudes than in the subsurface ocean at low latitudes could conceivably cause nonnegligible temperature gradients to arise on sloping isopycnal surfaces). This issue was addressed for temperature by *Harvey* [1995], who compared the oceanic heat uptake for two versions of his two–dimensional (2-D) (latitude-depth) ocean model, one formulated in diapycnal-isopycnal coordinates, the other formulated in vertical-horizontal coordinates. He found that as long as high-latitude convection was included in the model, there was very little difference between the two model versions. Since high-latitude convection is explicitly represented in the present 1-D model, this result suggests that the effective diffusion coefficient is unlikely to change dramatically during the transient response. *Joos et al.* [1997] examined the ability of a box-diffusion model, using an effective K, to simulate the transient uptake of anthropogenic CO_2 as simulated by a 3-D ocean general circulation model (GCM), and found little variation in the effective diffusion coefficient with time. However, the ocean GCM that they emulated used vertical-

Table 1. Approximate Mean Concentrations of Tracers in Low Latitude (30°) Surface Water (C_{LS}), High- Latitude (60°) Surface Water (C_{HS}), and in Subsurface (1000 m Depth) Low Latitude Water (C_{LSS}) [a]

Tracer	C_{LS}	C_{HS}	C_{LSS}	F_n	F_i	K_{eff}:K_n
DIC	1950	2050	2300	7.0×10^{-6}	1.7×10^{-6}	1.24:3.38
$\delta^{13}C$	-30	-60	-150	7.8×10^{-7}	1.9×10^{-7}	1.24:3.37
$\Delta^{14}C$	1.5	1.8	0.4	8.2×10^{-18}	2.0×10^{-18}	1.24:3.38
TALK	2270	2310	2350	1.6×10^{-6}	2.7×10^{-7}	1.17:2.67
TPO4	0.3	1.2	2.3	4.0×10^{-8}	7.3×10^{-9}	1.18:2.83
O_2	230	340	100	2.6×10^{-6}	1.6×10^{-6}	1.62:7.15

[a] Also given are the vertical tracer fluxes due to diapycnal (F_n) and isopycnal (F_i) mixing (assuming that K_n=0.2 cm^2 s^{-1}, K_i=100 m^2 s^{-1}, and δ=2 x 10^{-4}) and the ratio of the resultant effective vertical diffusion coefficient (K_{eff}) to the diapycnal diffusion coefficient (K_n) for the case in which K_i=1.0 x 10^2 m^2 s^{-1} (left column) or K_i=1.0 x 10^3 m^2 s^{-1} (right column).

horizontal rather than diapycnal-isopycnal coordinates, so their results are not applicable to the question at issue here. Although further work on this question is desirable, it is clear that the present model is an improvement over the classical 1-D upwelling-diffusion model.

2.4. Treatment of Convection

Convection is assumed to occur over a portion of the polar sea columns, with the fraction involved in convective mixing decreasing with depth according to

$$f_{conv}(z) = f_b + (f_t - f_b)[1 - \tanh(0.55z/\tau_{conv})] , \quad (6)$$

where τ_{conv} is a convective mixing scale depth, f_t is the fraction of the polar column involved in convection at the surface, and f_b is a lower limit to the fraction of the polar column involved in convective mixing at depth. The end-of-winter mixed layer depth throughout the regions of bottom water formation in the North Atlantic Ocean is typically 500-800 m [*Woods*, 1985, Figure 22], although mixing to a depth of 2000 m or more occurs on occasion in both the Labrador Sea and the Weddell Sea [*Killworth*, 1979]. Use of equation (6) produces a distribution of mixing depths such that the area involved in convection initially decreases slowly (as implied by the observations cited above), then drops to half of $f_t - f_b$ at a depth of τ_{conv}. We choose τ_{conv}=400 m.

Convective mixing in nature gradually progresses to successively greater depths as the cooling season progresses. However, the model is integrated using a 1-year time step. We have therefore adopted the following procedure: convective mixing is performed by first mixing the appropriate fraction of the first two model layers, then mixing a smaller fraction of the first three layers, and so on until convection has extended to the bottom of the column. This procedure in effect divides each 1-year time step into N ministeps that are distributed over the portion of the year where convection occurs, where N is the number of model layers (30). On each successive ministep, convective mixing involves a smaller fraction of the grid boxes but extends to a greater depth. At the end of the time step, a single mean tracer value is computed for each layer. In the case of O_2 and DIC, we allow for continuous exchange between the mixed layer and atmosphere during the convective mixing process, as explained in part 2. As will be seen in section 2.5, the inclusion of convective mixing within the upwelling – diffusion model framework has a significant effect on the transient surface climate response when a large decrease in the intensity of the thermohaline circulation is imposed. Use of the convective scheme presented here, with air-sea gas exchange as mixing proceeds to greater depths, is also particularly important to the successful simulation of the observed O_2 profile, as shown in part 2.

2.5. Temperature of Water Flowing Into the DPD

In the conventional UD model, the temperature of the water that leaves the mixed layer and upwells from the bottom of the ocean is prescribed. Here we have a separate polar domain that feeds the sinking bottom water, and its temperature is freely predicted. However, we must still prescribe the temperature of water that flows laterally into the downwelling polar domain (DPD) from the nonpolar domain. The simplest procedure would be to assume that the inflow temperature is equal to the temperature of the nonpolar domain. However, this results in excessively warm water entering the DPD. We define the downwelling polar domain as the region where the present – day mean annual mixed layer temperature is 2°C or less; this threshold was chosen because the warmest bottom water (in the North Atlantic region) today forms at 2°C. Thus the boundary between the polar and nonpolar domains coincides with the 2°C surface isotherm, so an alternative to using the nonpolar temperature as the inflow temperature is to prescribe an inflow temperature of 2°C (this is a less restrictive procedure than directly specify the temperature of bottom water formation, as in the conventional UD model). However, this is not entirely satisfactory because subsurface temperatures in the North Atlantic are warmer than the surface water, owing to the fact that surface water experiences direct cooling to the atmosphere, whereas the poleward flowing subsurface water does not. Thus we prescribe an inflow temperature T_i of 2°C at the surface but assume that the depression of the inflow temperature from the nonpolar temperature in a given layer decreases exponentially from the temperature depression found at the surface. That is,

$$Ti(z) = T(z) - [T(0) - Ti(0)]e^{-\frac{z}{\tau p}} , \quad (7)$$

where τ_p= 200 m. Use of equation (7) causes the subsurface water which flows into the polar domain to be 1°-2°C warmer than surface water, so that convective mixing produces an upward heat flux.

When the climate changes, the ratio of the warming of bottom water to the mixed layer warming is specified in the UD model (*Hoffert et al.* [1980] represented this ratio by the symbol π). Analogously, we can specify the ratio of the warming of the surface inflow ($T_i(0)$) to the surface mixed layer warming.

2.6. Control of Climate Sensitivity

The equilibrium atmospheric temperature response, ΔT_{eq}, to an external forcing, ΔR (such as doubling of atmospheric CO_2) is given by

$$\Delta T_{eq} = \frac{\Delta R}{\lambda} , \quad (8)$$

where λ is the radiative damping. Neither the classical UD model nor the quasi–one–dimensional (Q1D) model presented here have a temperature-surface albedo feedback, and if changes in the amount of atmospheric water vapor for purposes of solar radiation are suppressed for simplicity, then λ is equal to the coefficient B in the parameterization of infrared radiation to space,

$$L_{out} = A + BT_a . \quad (9)$$

Thus the model sensitivity to a CO_2 doubling can be set to any desired value through the choice of B.

3. Model Spin–up Using Base Case Parameter Values

3.1. Base Case Parameter Values

The model contains a number of parameters that can be adjusted, within observational limits, so as to obtain the best possible fit of the model spin–up state to observations. This tuning exercise involves consideration of not only temperature but of all the other model tracers (including the carbon isotope ratios) and is described in full in part 2 (where nontemperature variables are considered). The tunable parameters of interest here are A_o (which serves as a uniform scaling factor for the diapy-

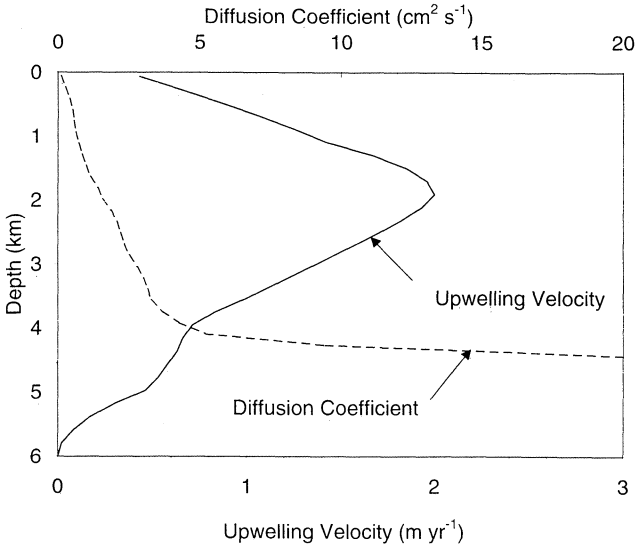

Figure 3. Vertical variation of the diapycnal diffusion coefficient used and of the upwelling velocity.

cnal diffusion coefficient), the magnitude and vertical variation in the upwelling velocity, and τ_p (of equation A3), which determines how the temperature of the water flowing into the downwelling polar domain from the nonpolar domain varies with depth. All of these parameters are constrained to within a factor of 2 or better by direct observations. The values for A_0 and τ_p, and the variation of w in the upper kilometres, can be refined by matching the model mean temperature profile to observations, as these are the only parameters that noticeably affect the mean temperature profile. Given the values of A_0, τ_p, and w deduced in this way, it turns out to be possible to find plausible values of the adjustable carbon cycle parameters that give an excellent fit to the steady state (preindustrial) vertical variation of the carbon cycle tracers. These parameter values can then be independently validated by comparing model-predicted and observed transient variations; as shown in part 2, the agreement is also excellent.

Figure 3 shows the vertical variation of w and $K_n(z)$ adopted here (the total K_x for all tracers are compared in part 2). The vertical variation in the w profile is similar to that implied by recent simulations with the Hamburg OGCM [*Drijfhout et al.*, 1996]. The $K_n(z)$ increases from 0.15 cm^2 s^{-1} at the base of the mixed layer to ~1.0 cm^2 s^{-1} at the 2 km depth and 20 cm^2 s^{-1} at the ocean bottom. Many observations indicate that the diapycnal diffusion coefficient (K_n) is ~0.1-0.2 cm^2 s^{-1} at the base of the mixed layer and increases with increasing depth [e.g., *Gregg*, 1987; *Schlitzer*, 1989; *Moum and Osborn*, 1986; *Ledwell et al.*, 1993]. *Moum and Osborn* [1986], in particular, obtained a value of 1.0 cm^2 s^{-1} at the 2 km depth, which agrees with our 2 km value. We use τ_p=200 m.

3.2. Spin–up Ocean Temperature Profile

The present model can be converted to the classical upwelling-diffusion model if the ocean is assumed to be at a constant depth of 4000 m everywhere, if vertically uniform K and w are imposed, if sinking water is assumed to flow directly from the nonpolar domain into the polar plume (shown to the right of Figure 1) without conditioning in the downwelling polar domain, if the upwelling flux in the upwelling polar domain is set to zero, and if convective mixing is suppressed in both polar domains. The conventional values for K and w in the upwelling diffusion model are 0.6 cm^2 s^{-1} and 4 m yr^{-1}, respectively [*Hoffert et al.*, 1980]. An intermediate model version can be created which is the same as the classical UD model, except that the K and w derived here are used in place of the conventional, vertically uniform values, and realistic bathymetry is used. This shall be referred to as the "Altered 1-D model."

Figure 4 compares the observed, global mean profile of ocean temperature (computed from *Levitus* [1982]) with that simulated by the classical UD model, the Altered 1-D model, and the present, quasi-one dimensional model (the Q1D model). The classical UD model fits the observations very well, by design. The equilibrium temperature profile in this case is given by

$$\theta(z) = \theta b + (T_{ML} - \theta b)e^{-z/\tau} , \qquad (10)$$

where $\theta(z)$ is the temperature at depth z, θ_b is the temperature of the downwelling water (which is prescribed in the classical UD model), T_{ML} is the global mean mixed layer temperature, and τ=K/w is a scale depth. The profile shown in Figure 4 was obtained using θ_b=274.15 K, T_{ML}=291.3 K (T_{ML} is predicted by the model), K= 0.6 cm^2 s^{-1}, and w =4 m yr^{-1}, giving τ=473 m. In the Altered 1-D model, τ varies with depth, increasing from 800 m at the base of the mixed layer to 2 km at the 2 km depth. Consequently, the temperature decreases less rapidly with depth in the upper ocean than in the classical model. This, combined with the very large diffusion coefficient in the lower ocean, causes the deep ocean temperature to be ~2 K warmer than the temperature of upwelling bottom water. As a result, the entire temperature profile is shifted toward warmer temperatures in the Altered 1-D model. However, once convection is allowed (as in the Q1D model), the entire ocean profile is cooled, resulting in a temperature profile close to observations and close to the classi-

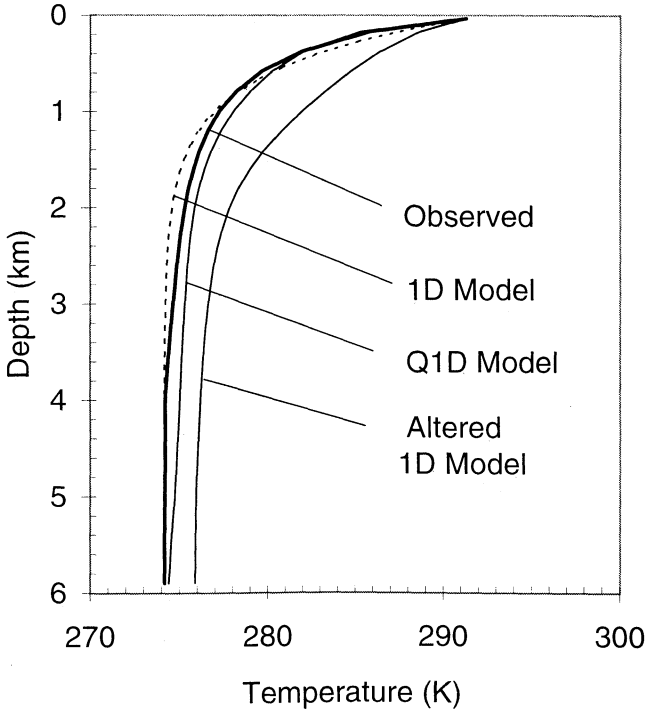

Figure 4. Comparison of the observed global mean variation in ocean temperature with the variation simulation using the conventional 1-D upwelling-diffusion model, the Altered 1-D model, and the Q1D model.

Table 2. Mixed Layer-to-Deep Ocean Heat Fluxes for the Classical Upwelling Diffusion (UD) Model, the Altered 1-D Model, and the Q1D Model [a]

Model	Diffusive Flux	Advective Flux	Convective Flux
1-D	7.498	-7.498	0.000
Altered 1-D	0.908	-0.908	0.000
Q1D	1.957	-0.516	-1.441

[a] Heat fluxes are given in W m^{-2}.

cal 1-D model. Thus the inclusion of convection allows us to utilize K_v and w values that are close to the directly observed or inferred values and which (as shown in part 2) are required in order to successfully simulate the other oceanic tracers.

Table 2 compares the mixed layer – deep ocean heat balance for the three model versions. Advection (by the thermohaline circulation, THC) transports heat upward, since the sinking polar water is colder than upwelling water at lower latitudes. Convection, where present, also transports heat upward, while the diffusive heat flux is downward. In the classical UD model, the diffusive and advective fluxes are relatively large because of the large K and near-surface w. These fluxes are much smaller in the other two models, a fact that is important to the transient surface temperature and sea level response to a collapse of the thermohaline circulation.

4. Transient Temperature and Sea Level Response

It is a robust result of coupled AOGCMs and coupled, 2-D atmosphere-ocean models that the thermohaline circulation (THC) weakens as the climate warms in response to anthropogenic greenhouse gas emission and may undergo a near-total collapse at some point (T.M.L. Wigley and L.D.D. Harvey, manuscript in preparation, 2001). Neither the classical UD model nor the Q1D model presented here can be used to predict how the THC will change, but they can be used to assess the impact of hypothetical THC changes on the transient temperature response, sea level rise, and oceanic storage of carbon. Changes in the THC in 1-D models could either be suddenly imposed or could arise through a prescribed feedback with surface climate. Here we compare the behavior of the classical upwelling-diffusion model, the Altered 1-D model, and the Q1D model to changes in the THC.

Prior to examining our temperature and sea level response results, we present the thermal expansion coefficient as a function of depth for the nonpolar domain in Figure 5 (we use the equation of state of *Friedrich and Levitus*, [1972]). Results are shown for the thermal expansion coefficient when all densities are calculated assuming an ocean depth of zero, when the pressure-dependence of density on pressure is included, and when the pressure dependence is included but the coefficient is multiplied by the ocean area as a fraction of the surface area. It is often assumed that thermal expansion in the deep ocean does not make an important contribution to sea level rise because the thermal expansion coefficient is much smaller at typical deep ocean temperatures (0°-2°C) than at temperatures in the upper thermocline. However, the thermal expansion coefficient increases strongly with increasing pressure. The net result is that thermal expansion coefficient is almost as large in the deep ocean (4-6 km depth) as it is in the upper thermocline. The sensitivity of sea level rise to deep ocean warming will be reduced owing to the smaller volume associated with a given depth interval than in the upper ocean. The net result of both the pressure and area dependencies is that changes in ocean temperature in the entire top 3-4 km of the ocean will have an important effect on the predicted sea level rise, as seen in Figure 5.

Figure 6 shows the surface temperature and sea level response when the THC is suddenly and completely shut off (i.e., when w is set to zero), while Figure 7 gives the profile of deep ocean temperature change in the new steady state. Since the THC causes a net upward heat transfer, a THC shutoff causes a transient surface cooling and a deep ocean warming. In the UD model, the deep ocean acquires an isothermal profile at a temperature equal to the mixed layer temperature. Thus the deep ocean warms by ~17 K, and the rise in sea level approaches 14 m. In the Altered 1-D model, impact of a THC collapse on the surface temperature is much less because the spin–up advective heat flux is much less (Table 2). However, the eventual deep sea warming and sea level rise are only slightly less. This is because both models move toward the same isothermal state when the THC collapses, but the Altered 1-D model starts from a deep ocean state that is 2 K warmer (Figure 4), so the deep ocean warming is 2 K less. The surface temperature response of the Q1D model is similar to that of the Altered 1-D model (Figure 6a) because the spin–up advective heat flux is comparable. However, the continued occurrence of convection serves to maintain a cold deep ocean even in the absence of thermohaline overturning. The new steady state profile is not an isothermal profile, and the mean deep ocean warming and sea level rise are dramatically less than for either of the other models (Figures 6b and 7).

Figures 8 and 9 compare the equilibrium model response to a sudden doubling of the atmospheric CO_2 concentration for cases with fixed THC and when the THC circulation weakens gradually in response to warming of the mixed layer. For these ex-

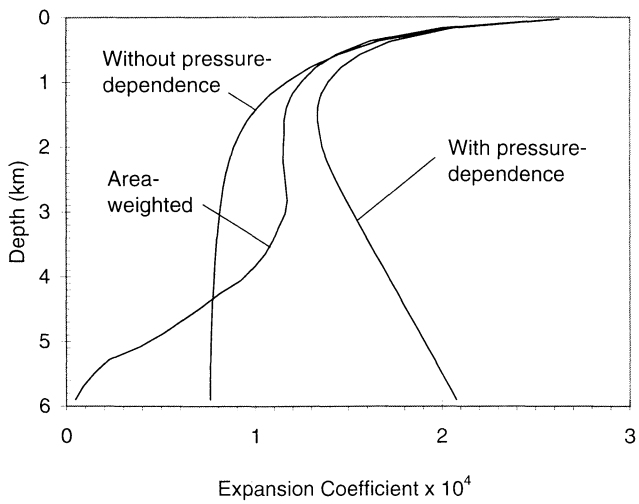

Figure 5. Variation of the thermal expansion coefficient with depth in the nonpolar domain for cases in which density is computed using the ambient pressure or neglecting the pressure dependence. Also given is the thermal expansion coefficient multiplied by the depth-varying ocean area as a fraction of the surface ocean area.

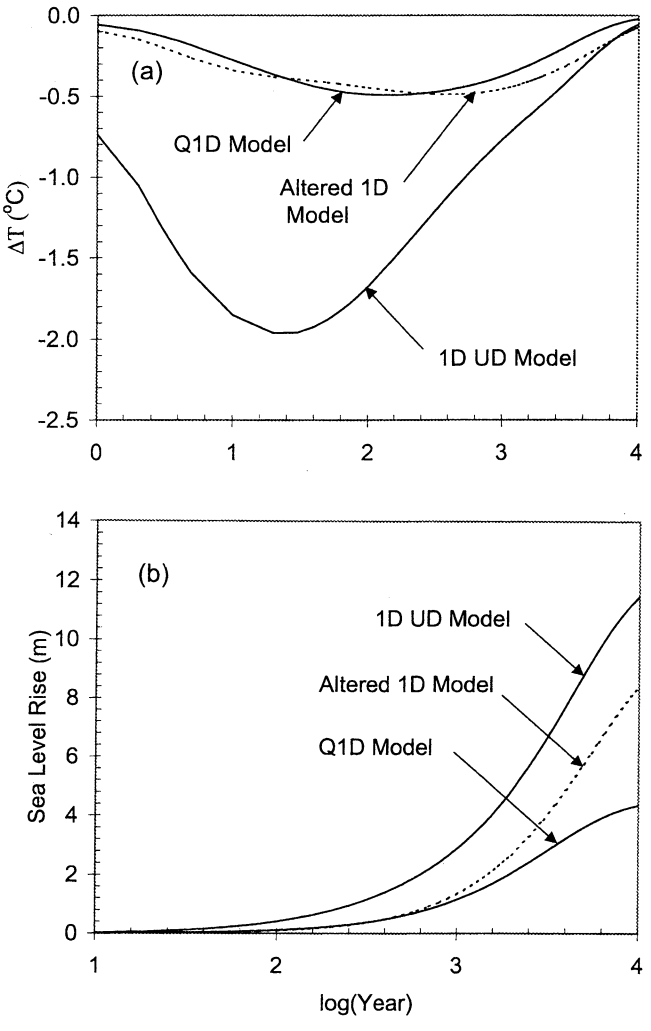

Figure 6. Response of the UD, Altered 1-D, and Q1D models to a sudden shut down of the thermohaline circulation. (a) Mixed layer temperature response; (b) sea level rise due to thermal expansion of sea water.

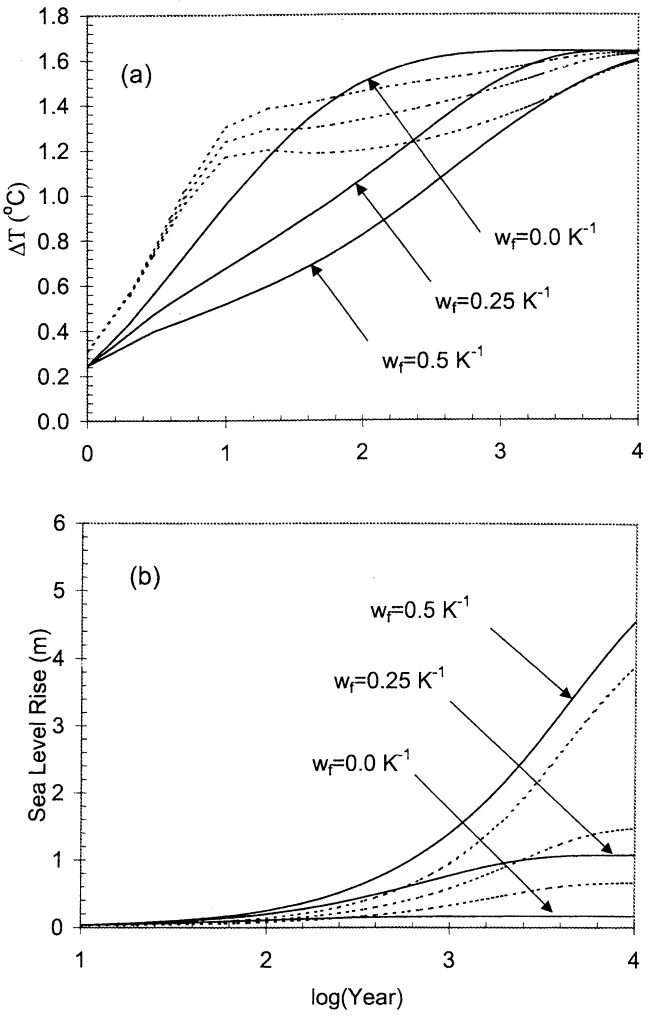

Figure 8. Response of the UD (solid lines) and Q1D (dashed lines) models to a sudden doubling of the atmospheric CO_2 concentration with fixed thermohaline circulation (w_f=0.0 K^{-1}) and with a climate-thermohaline circulation feedback (w_f=-0.25 and -0.50 K^{-1}). (a) Mixed layer temperature response; (b) sea level rise due to thermal expansion of sea water.

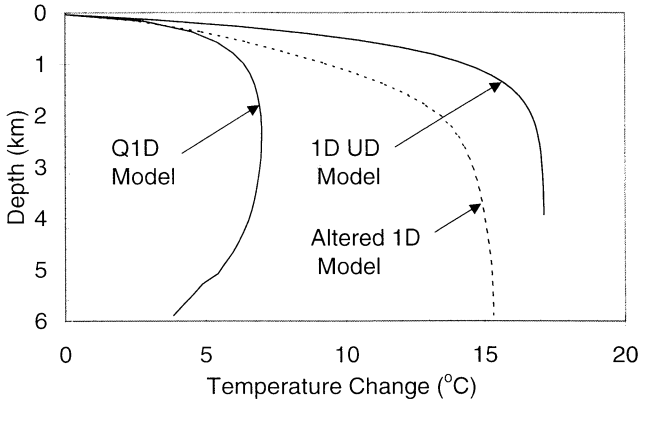

Figure 7. The profile of steady state global mean deep ocean temperature change following a sudden shut down of the thermohaline circulation for the UD, Altered 1-D, and Q1D models.

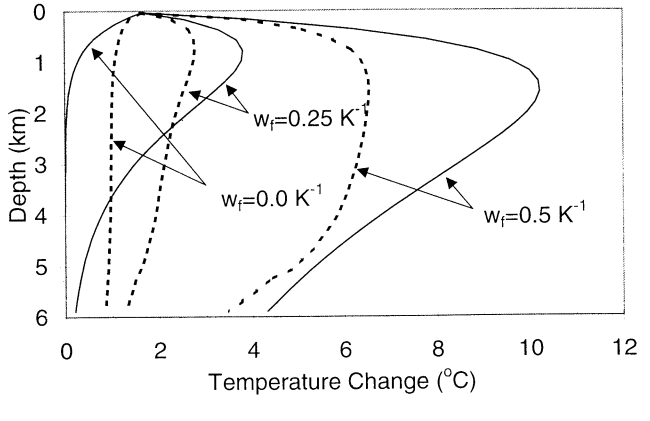

Figure 9. The profile of steady state global mean deep ocean temperature change following a sudden doubling of the atmospheric CO_2 concentrations for the UD (solid lines) and Q1D (dashed lines) models.

periments, an equilibrium surface-air atmospheric sensitivity of 2.0°C for a CO_2 doubling was chosen, and the THC intensity, I, was assumed to change according to

$$I = I_o(1 - w_f \Delta T_{ML}), \quad (11)$$

where I_o is the initial intensity and ΔT_{ML} is the mixed layer temperature change. In the UD model the temperature of bottom water formation (θ_b) was held constant, while the inflow temperature T_i was held constant in the Q1D model. Results are shown in Figures 8 and 9 for w_f=0.0, 0.25, and 0.5 K^{-1}, for the UD model (solid lines) and the Q1D model (dashed lines). In the absence of changes in the THC circulation, the temperature response of the Q1D model is initially faster than that of the UD model, owing to the smaller near-surface K_n in the Q1D model. In the UD model, with fixed THC and θ_b, the steady state temperature change exponentially decreases to zero with increasing depth (as can be inferred from equation (10)). In the Q1D model, there is some deep ocean warming due to the fact that the downwelling polar column warms even if there is no change in the inflow temperature. As a result, the integrated heat flow into the deep ocean for the Q1D model is greater than in the UD model. Since this heat flow retards the surface temperature increase, the surface temperature response in the UD model eventually overtakes that of the Q1D model, in spite of getting a slower start.

One might ask why the deep ocean warming in the Q1D model is not even larger than shown for the case with w_f=0.0 K^{-1}, since the polar sea temperature is presumably free to warm by an amount governed by the radiative damping to space (the coefficient B), which is the same in all domains. The reason the polar sea warming is limited is that the polar surface temperature is prevented from dropping below the freezing point of sea water (271 K), by resetting the temperature to 271 K when needed and making an energy-conserving adjustment to the nonpolar surface temperature (this mimics the net effect of what happens in nature through the formation and export of sea ice, and through the resulting depression of polar air temperatures, which will cause enhanced heat flow into the polar region). The initial effect of a warmer climate is to reduce the extent to which the polar surface temperature needs to be adjusted in order to keep it from dropping below 271 K. Only later does warming of the polar surface layer occur. This limits the bottom water warming for a CO_2 doubling to about half global the mean surface warming when the THC intensity is fixed.

A weakening of the THC as part of a climate feedback significantly slows the surface temperature response for the UD model (Figure 8a) and enhances the sea level rise (Figure 8b), owing to the fact that heat can penetrate into the deep ocean as the THC weakens. The effect of this feedback is much less for the Q1D model, owing to the fact that the deep ocean temperature profile is less sensitive to changes in the THC intensity in the Q1D model (Figure 9).

The case w_f=-0.5 K^{-1} corresponds to a reduction in the THC by ~80%. The equilibrium sea level rise for this case using the Q1D model (4.3 m) is substantially larger than the sea level rise of ~1.3 m obtained by *Knutti and Stocker* [2000] for a complete shut down of North Atlantic deep water formation and a global mean atmospheric temperature increase of 2.0°C. However, in their study, the rate of formation of Antarctic Bottom Water was fixed and the deep ocean warming was substantially less than in our simulations (R. Knutti, personal communication, 2001). The large sea level rise obtained with our model is a direct consequence of the relatively large (4°-6°C) deep ocean warming.

In the above experiments with the classical UD model, the average temperature at which bottom water forms was held constant. As previously noted, *Hoffert et al.* [1980] used the symbol π to represent the ratio of bottom water warming to global mean mixed layer warming. As discussed by *Harvey and Schneider* [1985], there are plausible conditions under which π could be slightly negative, zero, or positive. Figures 10 and 11 compare the UD and Q1D models for cases in which π=0.0 (as above) or π=1.0, with fixed THC intensity (in the Q1D model, π governs changes in the surface inflow temperature, T_i). Since a warmer downwelling water results in more heat flow into the deep ocean, use of π=1.0 slows down the surface temperature response and enhances the deep ocean warming and associated sea level rise compared to the case with π=0.0 in the classical UD model. However, the choice of π has negligible effect on the surface temperature response and only a small effect on the deep ocean temperature response in the Q1D model. This is because the temperature of bottom water formation is free to warm even with π=0.0, but the warming is more strongly controlled by the initial implicit presence of sea ice (the surface

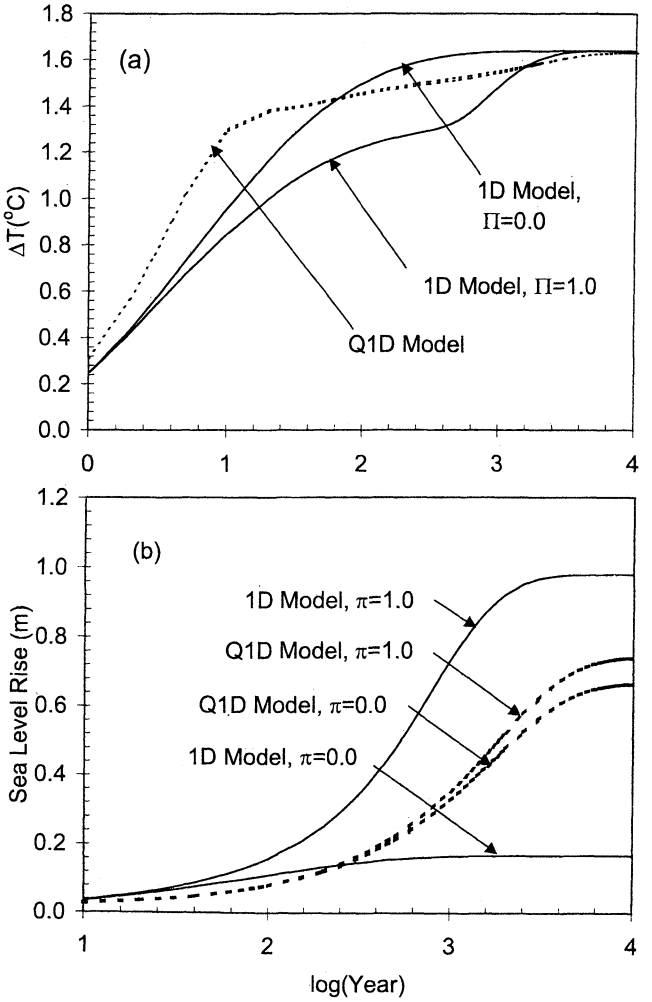

Figure 10. Response of the UD (solid lines) and Q1D (dashed lines) models to a sudden doubling of the atmospheric CO_2 concentration with fixed thermohaline circulation (w_f=0.0 K^{-1}) for cases where π=0.0 or π=1.0 See text for details. (a) Mixed layer temperature response; (b) sea level rise due to thermal expansion of sea water.

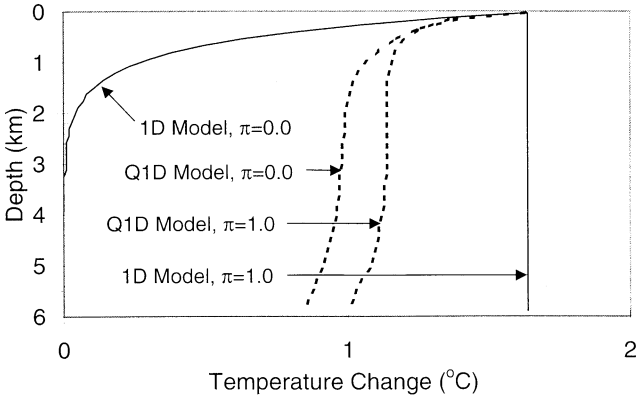

Figure 11. The profile of steady state global mean deep ocean temperature change following a sudden doubling of the atmospheric CO_2 concentrations for the UD (solid lines) and Q1D (dashed lines) models.

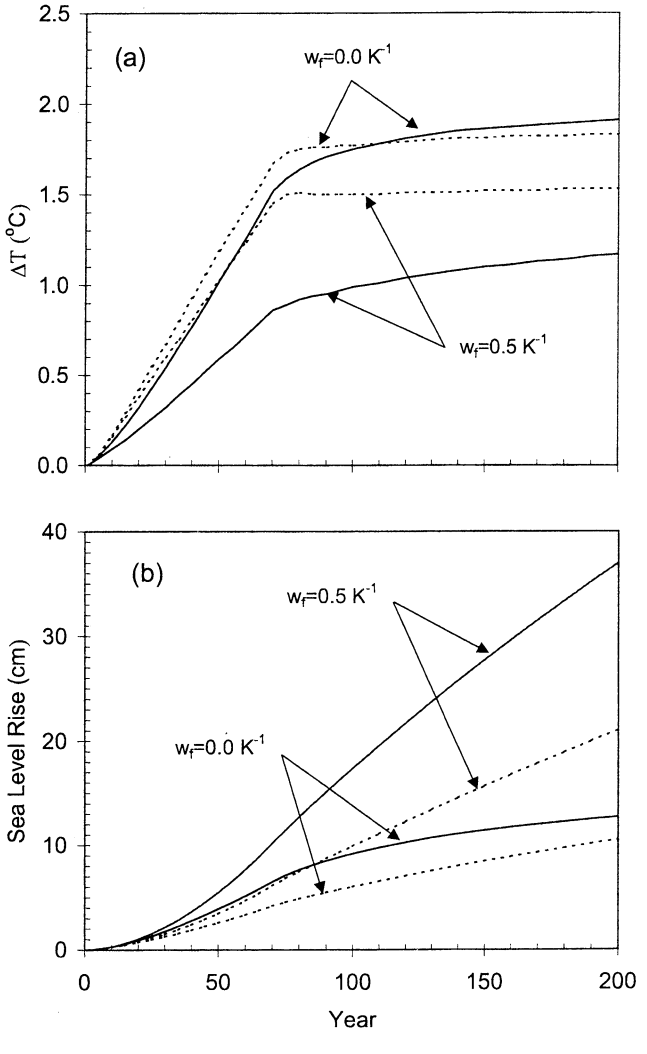

Figure 12. (a) Atmospheric temperature response (for a CO_2 doubling sensitivity of 2.0°C) and (b) sea level response to a 1% per year compounded increase in the CO_2 concentration until year 70 for the UD and Q1D model with fixed and variable THC intensity.

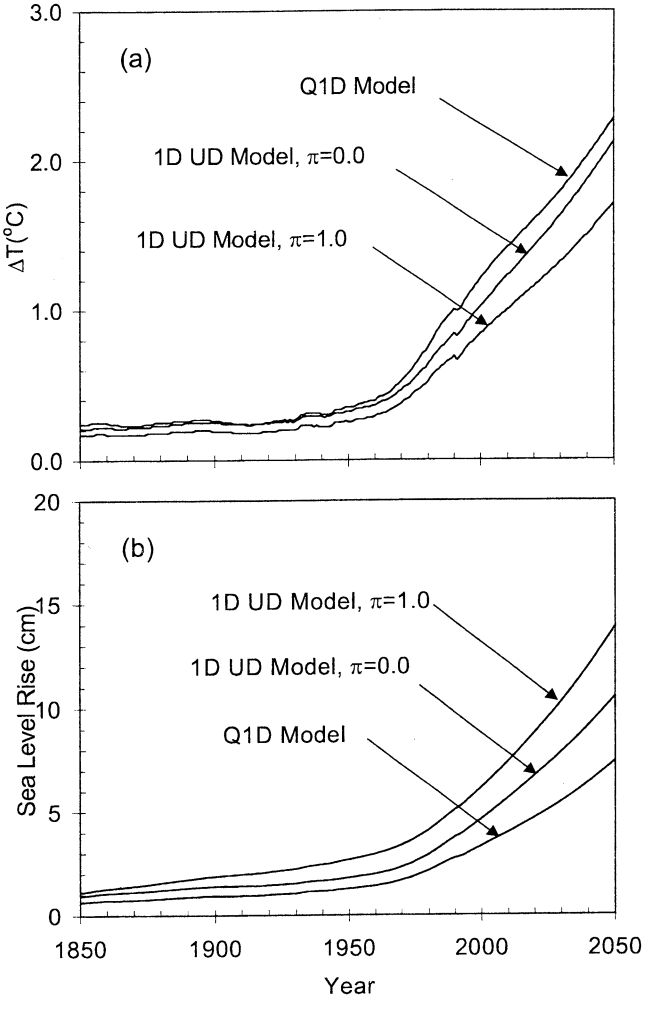

Figure 13. (a) Atmospheric temperature response (for a CO_2 doubling sensitivity of 3.0°C) and (b) sea level response to a combination of greenhouse gas and aerosol radiative forcing, for the UD model with π=0.0 or π=1.0, and for the Q1D model.

temperature had tended to drop below 271 K) than by changes (or lack thereof) in the inflow temperature.

Figures 12 and 13 compare the response of different model versions to a gradual increase in forcing. Figure 12 shows the response to a 1% per year (compounded) CO_2 increase until a doubling, at year 70, for cases with fixed THC and with w_f=0.5 K^{-1}. The rapid weakening of the THC has an early and dramatic effect on the surface temperature response of the UD model, as in the case of a step function CO_2 increase (compare Figures 8a and 12a). The effect is much smaller in the Q1D model. Figure 13 shows the response to a realistic historical and future scenario of net anthropogenic radiative forcing, in which the cooling effect of aerosols offsets 40% of the heating due to well-mixed greenhouse gases in 1990 (see Harvey and Kaufmann, 2002, for details). The transient warming of the UD model with π=1.0 is ~20% slower than with π=0.0. Although the Q1D model responds with the equivalent of π=0.5 by 2100 (bottom water warming reaches half of the global mean surface warming by 2100), the Q1D responds almost 10% faster than the UD model with π=0.0. This is due to the much smaller upper ocean K, which is only partly compensated by the smaller upwelling velocity (as explained by *Harvey and Schneider*, [1985], a

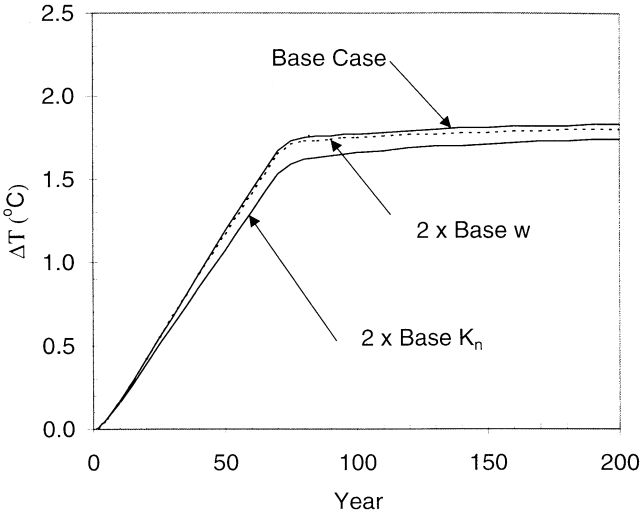

Figure 14. Effect on the transient atmospheric temperature response of the Q1D model when either the vertical diffusion coefficient (K_n) or the upwelling velocity (w) are doubled, for CO_2 doubling by year 70 and ΔT_{2x} =2.0°C.

stronger upwelling gives a faster transient response because the downward diffusing thermal perturbation is more strongly advected back into the mixed layer). Although the bottom water warming of the Q1D model is intermediate between that of the UD model with π=0.0 and 1.0, the sea level rise (Figure 13b) is less than for either UD model version. This must be due to less warming in the upper ocean due to the smaller upper-ocean K. As seen from Figure 13, faster transient surface warming is consistently associated with a smaller sea level rise (for a given climate sensitivity), since faster surface warming implies less heat flow into the subsurface ocean.

The UD model has been used in the past to infer the climate sensitivity by fitting model-simulated historical temperature changes to the observed temperature variation using various combinations of uncertain anthropogenic and natural radiative forcings [i.e., *Santer et al.*, 1996, section 8.4.1.3). The faster transient response of the Q1D model than UD model implies that the Q1D model will require a somewhat smaller set of climate sensitivities in order to fit the observed temperature variations.

Figure 14 shows the sensitivity of the Q1D model transient atmospheric temperature response to a doubling of K_n or of w. A doubling of w has a negligible effect on the transient response. This in contrast to the classical UD model, where doubling w causes a 5% faster response. The effect of doubling w on the transient response of the Altered 1-D model is also negligible. The insensitivity of the Q1D model to doubled w must be related to fact that w only gradually increases with increasing depth in the Q1D model, in contrast to the classical UD model, so that the upward advection of the downward diffusing thermal anomaly (which gives the faster transient response in the classical UD model) is very weak. The effect of a doubling of K_n is to slow the transient response by ~10%.

Figure 15 compares the global averaged surface – air temperature response of the Q1D model and the energy balance climate model–2-D ocean model of *Harvey* [1992], when driven with the radiative forcing due to the historical increase in greenhouse gases (as given by *Harvey and Kaufmann* [2001]). The vertical variation in the 2-D model of the flux-weighted vertical diffusion coefficient, and in the thermohaline upwelling velocity, are not exactly the same as adopted in the Q1D, but differ by up to 20%. For the comparison shown in Figure 15, the K and w values in the Q1D model were adjusted to be the same in the 2-D model (since altering the k and w in the 2-D model to exactly match those in the 1-D model is not easy). In both models, the global mean equilibrium atmospheric warming for a CO_2 doubling (ΔT_{2x}) can be prescribed. It can be seen that the Q1D model almost exactly replicates the behavior of the 2-D model, when both models are given equal climate sensitivities ranging from ΔT_{2x}=1.0°C to ΔT_{2x}=5.0°C.

5. Concluding Comments

In this paper we have presented the climate part of what is essentially a 1-D coupled climate-carbon cycle model. The only departure from the model's 1-D nature arises from the fact that we resolve two separate polar sea regions. In one of the polar regions, bottom water is conditioned by interaction with the atmosphere, lateral exchanges, and convective mixing, and is then injected into the deep ocean. In the other polar region, upwelling water enters from intermediate depths. The most important differences between this model and the classical upwelling-diffusion model from a climate-simulation point of view are (1) the use of a much smaller vertical diffusion coefficient in the upper ocean, (2) a weaker upwelling velocity, especially in the upper ocean, and (3) the occurrence of convective mixing of heat in the polar domains.

The transient surface temperature response and the transient and steady state deep ocean temperature and sea level response of the present model to a change in the intensity of the thermohaline circulation (either suddenly imposed or as part of a climate feedback) is significantly different from the widely used upwelling-diffusion model. In particular, a sudden collapse of the THC has a much smaller transient effect on the surface temperature, and the ultimate deep ocean warming and sea level

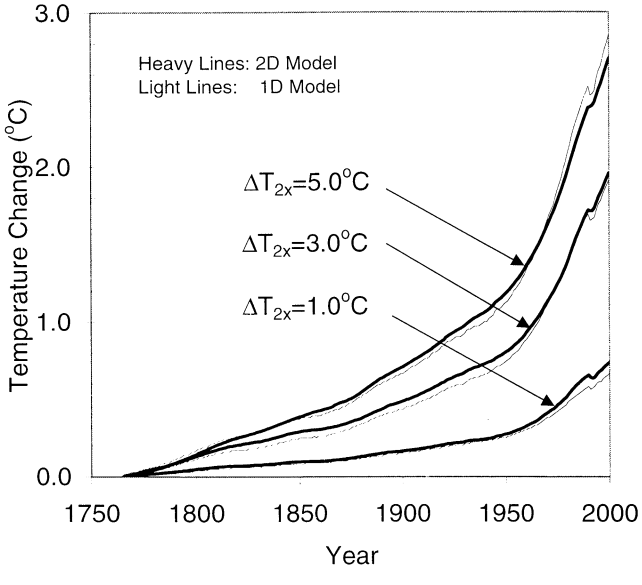

Figure 15. Comparison of the global mean atmospheric temperature response of the Q1D model and of the 2-D ocean model of Harvey (1992), when driven with the radiative forcing due to the historical buildup of greenhouse gases, for climate sensitivities ΔT_{2x} ranging from 1.0° to 5.0°C.

rise are much less (a 5 m sea level rise rather than a 12-14 m rise). The smaller effects obtained with the present model would appear to be more realistic. The transient temperature response to the historical variation in radiative forcing in faster for the Q1D model than for the UD, while the associated sea level rise due to thermal expansion is smaller. The faster surface temperature response in turn implies that the climate sensitivities that are consistent with the observed temperature variation during the past 140 years are ~10% smaller than what would be deduced using the classical UD model.

Appendix A: Governing Equations For the Oceanic Component

The mixing processes and model structure depicted in Figure 1 lead to equations of the following form for the concentration of tracer X in the nonpolar domain:

$$h\frac{dX}{dt} = w(h)X(h) + K_x(h)\frac{\partial X}{\partial z}|_{z=h} + h\left(\frac{F_D(h)}{\gamma(h)} + S_{\mathrm{DPD}}(h) + S_{\mathrm{UPD}}(h) + B_{ML}\right) + R + F_{as} \quad \text{(A1)}$$

for the mixed layer, and

$$\gamma(z)\frac{\partial X}{\partial t} = \frac{\partial}{\partial z}\left(\gamma(z)w(z)X(z) + \gamma(z)K_x(z)\frac{\partial X}{\partial z}\right) + \frac{F_D(z)}{\gamma(z)} + S_{\mathrm{DPD}}(z) + S_{\mathrm{UPD}}(z) + B(z) \quad \text{(A2)}$$

for the ocean below the mixed layer. Here, z is ocean depth (increasing downward), h is the mixed layer depth, X is the depth-dependent concentration in the nonpolar domain, $\gamma(z)$ is the nonpolar ocean area at depth z as a fraction of the nonpolar ocean surface area, K_X is an effective vertical diffusion coefficient appropriate for tracer X, w is the upwelling velocity in the nonpolar domain required to balance the net vertical mass flux in the two polar domains, F_D represents the effect of diffusive mixing between the polar and nonpolar domains, R represents river inputs, B_{ML} represents the effect of biological production in the mixed layer and $B(z)$ the effect of decay or dissolution below the mixed layer, F_{as} is the flux density from the atmosphere to the ocean, and S_{DPD} and S_{UPD} are source or sink terms representing the effect of lateral flow of water into or from the downwelling and upwelling polar columns, respectively. Here X can represent temperature, DIC (which is tracked separately for each carbon isotope), TALK, TPO4, or oxygen. In the case of temperature, $F_{as}/(\rho c_p)$ is the air-sea heat flux (W m^{-2}), while for alkalinity and phosphate, F_{as}=0. In the case of oxygen, the mixed layer concentration is reset to 3% greater than the saturation value at the end of each time step, and F_{as} is the implicit flux required to maintain 3% supersaturation. For alkalinity and phosphate the river term R represents the long-term geological recycling via erosion of continents needed to balance the model-computed rates of carbonate and phosphate burial, respectively. For carbon the river term is equal to the rate of net organic carbon burial only, as net carbonate burial of carbon is balanced by a volcanic CO_2 flux to the atmosphere. For temperature, R, B_{ML}, and $B(z)$ are all zero.

The equations governing the tracer concentration in the downwelling polar domain below the mixed layer are

$$A(z)_{dp}\frac{\partial \mathrm{X}_{dp}}{\partial t} = \frac{\partial F_{dp}}{\partial z}(\mathrm{X}_i - \mathrm{X}_{dp}) + A(z)_{dp}\left(F_C(z) - \frac{F_D(z)}{\gamma(z)_{dp}} + B(z)\right), \frac{\partial F_{nh}}{\partial z} > 0 \quad \text{(A3a)}$$

$$A(z)_{dp}\frac{\partial \mathrm{X}_{dp}}{\partial t} = -\frac{\partial F_{dp}}{\partial z}(\mathrm{X}_{plume} - \mathrm{X}_{dp}) + A(z)_{dp}\left(F_C(z) - \frac{F_D(z)}{\gamma(z)_{dp}} + B(z)\right), \frac{\partial F_{nh}}{\partial z} < 0 \quad \text{(A3b)}$$

where A_{dp} is the area of the downwelling polar domain, F_{dp} is the downwelling plume flux (seen to the right of the downwelling column in Figure 1), F_D and B are as previously defined, and F_C represents the effect of convective mixing. For the mixed layer, additional terms representing river input and air-sea exchange are present. Where $\partial F_{dp}/\partial z > 0$ (in the upper ocean), lateral flow is from the nonpolar domain, through the downwelling polar domain, and into the sinking plume. During its transit through the downwelling polar domain, the inflowing water is conditioned through air-sea interaction, convective mixing, and biological processes. Where $\partial F_{dp}/\partial z > 0$ (in the lower ocean), water detrains from the sinking plume at the mean plume concentration of X_{plume} and passes through the downwelling polar column into the nonpolar domain (X_{plume} is constant below the depth where detrainment begins). The corresponding source-sink term appearing in equation (A2) is

$$S_{dp}(z) = -\frac{\mathrm{X}_i}{A_{np}}\frac{\partial F_{dp}}{\partial z}, \frac{\partial F_{dp}}{\partial z} > 0 \quad \text{(A4a)}$$

$$S_{dp}(z) = -\frac{\mathrm{X}_{dp}}{A_{np}}\frac{\partial F_{dp}}{\partial z}, \frac{\partial F_{dp}}{\partial z} < 0\ , \quad \text{(A4b)}$$

where $A_{dp}(z)$ is the area of the nonpolar domain.

In the case of the upwelling polar column, the mass flux is assumed to occur within the column itself rather than concentrated in a boundary layer plume. Recalling that z increases downward, this leads to equations of the form

$$A(z)_{up}\frac{\partial \mathrm{X}_{up}}{\partial t} = -\frac{\partial F_{up}}{\partial z}(\mathrm{X}_{np} - \mathrm{X}_{up}) + A(z)_{UP}\left(F_C(z) - \frac{F_D(z)}{\gamma(z)_{up}} + B(z)\right), \frac{\partial F_{up}}{\partial z} < 0 \quad \text{(A5a)}$$

for the lower ocean, where entrainment occurs, and

$$A(z)_{up}\frac{\partial \mathrm{X}_{up}}{\partial t} = \frac{\partial}{\partial z}(F_{up}\mathrm{X}_{up}) + A(z)_{up}\left(F_C(z) - \frac{F_D(z)}{\gamma(z)_{up}} + B(z)\right), \frac{\partial F_{up}}{\partial z} > 0 \quad \text{(A5b)}$$

for the upper ocean, where detrainment occurs. The corresponding source/sink term, $S_{\mathrm{UP}}(z)$, is given by

$$S_{up}(z) = \frac{\mathrm{X}_{up}}{A_{np}}\frac{\partial F_{up}}{\partial z}, \frac{\partial F_{up}}{\partial z} < 0 \quad \text{(A6a)}$$

$$S_{up}(z) = \frac{X_{up}}{A_{np}} \frac{\partial F_{up}}{\partial z}, \frac{\partial F_{up}}{\partial z} > 0. \quad \text{(A6b)}$$

The tracer flux due to lateral mixing between the polar and nonpolar domains is assumed to be directly proportional to the concentration difference. That is,

$$F_D = \alpha(X_{dp} - X_{np}) \quad \text{(A7)}$$

in the case of the flux between the nonpolar and downwelling polar domain, where α is an exchange coefficient whose value is discussed below.

The value of the lateral mixing coefficient, α, is determined by assuming that lateral mixing represents isopycnal diffusion. In that case, $\alpha \approx K/\Delta s^2$, where $\Delta s \approx 6000$ km is the spatial scale over which most of the polar-to-non-polar tracer difference occurs. Observations indicate that the isopycnal (or horizontal) diffusion coefficient is of the order of 10^2 m^2 s^{-1} below the mixed layer [*Hogg*, 1987; *Jenkins*, 1991], which implies that $\alpha \approx 0.0001$ yr^{-1}. If heat transport within the mixed layer is modelled as diffusion, a typical diffusion coefficient value is 1.8 x 10^4 m^2 s^{-2} [*Harvey*, 1988], so that $\alpha \approx 0.015$ yr^{-1}. It is assumed here that α decreases exponentially from a mixed layer value of 0.015 yr^{-1} to a deep ocean value of 0.0001 yr^{-1}. The deep ocean value of α adopted here is an order of magnitude smaller than that used by *Shaffer and Sarmiento* [1995]. They interpreted their lateral exchange coefficient as representing the effect of hypothetical deep recirculation cells having a total transport of about 86 Sv. This interpretation in turn was used to justify the small circulation (5 Sv) associated with their upwelling velocity (0.6 m yr^{-1}). The model equations are solved using a non-uniform grid with 30 layers, such that the grid spacing is smallest at the top of the ocean and increases gradually with depth.

Appendix B: Solution Algorithm

The climate model consists of three atmospheric boxes (over the nonpolar and two polar domains), three mixed layer boxes, and the underlying deep ocean columns. The equations governing the atmospheric and mixed layer temperatures are

$$R_a \frac{dT_a}{dT} = Q_a^* + L\uparrow + H + L - L\downarrow - L_{out} + F_{ha} \quad \text{(B1)}$$

and

$$R_{ML} \frac{dT_{ML}}{dt} = Q_s^* - L\uparrow - H - L + L\downarrow + F_{hs} + F_v, \quad \text{(B2)}$$

respectively. Here, Q_a* and Q_s* are the rate of absorption of solar energy in the atmosphere and surface, respectively, $L\uparrow$ and $L\downarrow$ are the upward and downward infrared fluxes at the surface, respectively, H and L are the vertical sensible and latent heat fluxes, respectively, L_{out} is the infrared emission to space, F_{ha} and F_{hs} represent the effects of horizontal heat exchange, and F_v is the effect of heart exchange between the mixed layer and underlying ocean. Equations (B1) and (B2) are solved using 1-year time steps by linearizing them and recasting them in the form:

$$R_a \frac{d\Delta T_a}{dt} = \left(\frac{dH}{dT_a} + \frac{dL}{dT_a} - \frac{dL\downarrow}{dT_a} - \frac{dL_{out}}{dT_a}\right)\Delta T_a + \left(\frac{dH}{dT_s} + \frac{dL}{dT_s} + \frac{dL\uparrow}{dT_s}\right)\Delta T_s + B_a \quad \text{(B3)}$$

and

$$R_{ML} \frac{d\Delta T_{ML}}{dt} = -\left(\frac{dH_a}{dT_a} + \frac{dL}{dT_a} - \frac{dL\downarrow}{dT_a}\right)\Delta T_a - \left(\frac{dH}{dT_s} + \frac{dL}{dT_s} + \frac{dL\uparrow}{dT_s}\right)\Delta T_a + B_{ML}, \quad \text{(B4)}$$

where ΔT_a and ΔT_{ML} are the temperature changes since the beginning of the time step, $B_a = Q_a^* + F_{ha} + (L\uparrow + H + L - L\downarrow - L_{out})_o$, $B_s = Q_s^* + F_{hs} + F_v - (L\uparrow + H + L - L\downarrow)_o$, and the subscript o denotes values at the beginning of the time step. Q_a*, Q_s*, F_{ha}, and F_{hs} are assumed to constant within a time step.

The procedure for determining atmospheric, mixed layer, and deep ocean temperature changes is as follows: equations (B3) and (B4) are solved analytically using the values of all the terms appearing in B_a and B_{ML} as computed at the beginning of the current time step or at the end of the previous time step. Next, equation (A3a) and (A4a), governing the upper layers of the downwelling polar column, are analytically integrated over a 1-year time step. The integrated outflow of tracer from each layer l into the sinking plume is given by $\Delta F_{dp}\Delta t X_l - \Delta z_l A_{dp} \Delta X_{dp}$, where ΔF_{dp} is the increase in F_{dp} from the bottom to the top of the layer, Δt is the time step length, and ΔX_{dp} is the analytically determined change in X_{dp}. The contributions to the polar plume from each layer are assumed to be thoroughly mixed, producing a mean plume concentration, X_{plume}, which is then used in the analytic solution to equations (A3b) for the lower layers of the polar column, into which detrainment of the plume occurs. The time-integrated outflow from the downwelling polar domain to the nonpolar domain is the source term $S_{dp}(z)$ appearing in equation (A2) for the lower layers, and is given by $\Delta F_{dp}\Delta t X_{\text{plume}} - \Delta z_l A_{dp} \Delta X_{dp}$. The sink term $S_{dp}(z)$ for the upper layers is given by $\Delta F_{dp}\Delta t C_i$. Next, equations (A5a) and (A5b), governing the upwelling polar domain, are solved analytically beginning with the lowest layer and working upward. The source-sink term $S_{up}(z)$ is determined in a manner similar to that used to determine $S_{dp}(z)$. Having determined $S_{dp}(z)$ and $S_{up}(z)$ for all layers, equation (A2) is solved using the Crank-Nicholson scheme with a 1-year time step. However, the new mixed layer tracer values are not kept; rather, as explained above, the mixed layer tendency is determined and used as a forcing term in the analytic solution to the air-sea exchange equations.

Acknowledgment. This research was supported by NSERC grant OGP0001413.

References

Bacastow, R., and E. Maier-Reimer, Ocean circulation model of the carbon cycle, *Clim. Dyn., 4*, 95-125, 1990.

Bryan, F., Parameter sensitivity of primitive equation ocean general circulation models, *J. Phys. Oceanogr., 17*, 970-985, 1987.

Döös, K., and D.J. Webb, The Deacon Cell and other meridional cells of the Southern Ocean, *J. Phys. Oceanogr., 24*, 429-442, 1994.

Drijfhout, S., C. Heinze, M. Latif, and E.M. Maier-Reimer, Mean circulation and internal variability in an ocean primitive equation model, *J. Phys. Oceanogr., 26*, 559-580, 1996.

Friedrich, H., and S. Levitus. An approximation to the equation of state for sea water suitable for numerical ocean models, *J. Phys. Oceanogr., 2*, 514-517, 1972.

Gaffin, S.R., M.I. Hoffert, and T. Volk, Nonlinear coupling between surface temperature and ocean upwelling as an agent in historical climate variations, *J. Geophys. Res., 91*, 3944-3950, 1986.

Gargett, A, Vertical eddy diffusivity in the ocean interior, *J. Mar. Res., 42*, 359-393, 1984.

Gregg, M.C., Diapycnal mixing in the thermocline: A review, *J. Geophys. Res., 92*, 5249-5286, 1987.

Harvey, L.D.D., A semianalytic energy balance climate model with explicit sea ice and snow physics, *J. Clim., 1*, 1065-1085, 1988.

Harvey, L.D.D., A two-dimensional ocean model for long-term climatic simulations: Stability and coupling to atmospheric and sea ice models, *J. Geophys. Res., 97*, 9435-9453, 1992.

Harvey, L.D.D., Impact of isopycnal diffusion on heat fluxes and the transient response of a two-dimensional ocean model, *J. Phys. Oceanogr., 25*, 2166-2176, 1995.

Harvey, L.D.D., Polar boundary plumes and bottom water formation: A missing element in ocean general circulation models, *J. Geophys. Res., 101*, 20799-20808, 1996.

Harvey, L.D.D., A quasi-one-dimensional coupled climate-carbon cycle model, 2, The carbon cycle component, *J. Geophys. Res.*, this issue.

Harvery, L.D.D., and R. Kaufmann, Simultaneously constraining climate sensitivity and aerosol radiative forcing, *J. Clim.* (submitted).

Harvey, L.D.D., and S.H. Schneider, Transient climatic response to external forcing on 100-104 year time scales, 1, Experiments with globally averaged coupled atmosphere and ocean energy balance models, *J. Geophys. Res., 90*, 2191-2205, 1985.

Harvey, L.D.D., J. Gregory, M. Hoffert, A. Jain, M. Lal, R. Leemans, S. Raper, T. Wigley, and J. de Wolde, *An Introduction to Simple Climate Models Used in the IPCC Second Assessment Report, Tech. Pap.* 2, 53 pp., Intergovernmental Panel on Clim. Change, Geneva, 1997.

Hoffert, M.I., A.J. Callegari, and C.T. Hsieh, The role of deep sea heat storage in the secular response to climate forcing, *J. Geophys. Res., 85*, 6667-6679, 1980.

Hoffert, M.I., A.J. Callegari, and C.T. Hsieh, A box-diffusion carbon cycle model with upwelling, polar bottom water formation and a marine biosphere, in *Carbon Cycle Modelling, SCOPE 16*, edited by B. Bolin, pp. 287-305, John Wiley, New York, 1981.

Hogg, N.G., A least-squares fit of the advective-diffusive equations to Levitus Atlas data, *J. Mar. Res., 45*, 347-375, 1987.

Jain, A., H.S. Kheshgi, M.I. Hoffert, and D.J. Wuebbles, Distribution of radiocarbon as a test of global carbon cycle models, *Global Biogeochem. Cycles, 9*, 153-166, 1995.

Jain, A.K., H.S. Kheshgi, and D.J. Wuebbles, A globally aggregated reconstruction of cycles of carbon and its isotopes, *Tellus, Ser. B 48*, 583-600, 1996.

Jenkins, W.J., Determination of isopycnal diffusivity in the Sargasso Sea, *J. Phys. Oceanogr., 21*, 1058-1061, 1991.

Joos, F., J.C. Orr, and U. Siegenthaler, Ocean carbon transport in a box-diffusion versus a general circulation model, *J. Geophys. Res., 102*, 12,367-12,388, 1997.

Joos, F., G.K. Plattner, T.F. Stocker, O. Marchal, and A. Schmittner, Global warming and marine carbon cycle feedbacks on future atmospheric CO2, *Science, 284*, 464-467, 1999.

Kattenburg, A., F. Giorgi, H. Grassl, G.A. Meehl, J.F.B. Mitchell, R.J. Stouffer, T. Tokioka, A.J. Weaver, and T.M.L. Wigley, Climate models - projections of future climate, in *Climate Change 1995: The Science of Climate Change*, edited by J.T. Houghton, et al., pp. 285-357, Cambridge Univ. Press, New York, 1996.

Kelly, P.M. and T.M.L. Wigley, Solar cycle length, greenhouse forcing and global climate, *Nature, 360*, 328-330, 1992.

Kheshgi, H.S., B.P. Flannery, and M.I. Hoffert, Marine biota effects on the compositional structure of the world oceans, *J. Geophys. Res., 96*, 4957-4969, 1991.

Killworth, P.D., On "Chimney" formations in the ocean, *J. Phys. Oceanogr., 9*, 531-554, 1979.

Knutti, R., and T.F. Stocker, Influence of the thermohaline circulation on projected sea level rise, *J. Clim., 13*, 1997-2001, 2000.

Ledwell, J.R., A.J. Watsoon, and C.S. Law, Evidence for slow mixing across the pycnocline from an open-ocean tracer-release experiment, *Nature, 364*, 701-703, 1993.

Levitus, S., *Climatological Atlas of the World Ocean, Prof. Pap. 13*, 173 pp., Natl. Oceanic and Atmos. Admin., Washington, D.C., 1982.

Moum, J.N., and T.R. Osborn, Mixing in the main thermocline, *J. Phys. Oceanogr., 16*, 1250-1259, 1986.

Oeschger, H., U. Siegenthaler, U. Schotterer, and A. Gugelmann, A box diffusion model to study the carbon dioxide exchange in nature, *Tellus, 27*, 168-192, 1975.

Raper, S.C.B., and U. Cubasch, Emulation of the results from a coupled general circulation model using a simple climate model, *Geophys. Res. Let., 23*, 1107-1110, 1996.

Santer, B.D., T.M.L. Wigley, T.P. Barnett, and E. Anyamba, Detection of climate change and attribution of causes, in *Climate Change 1995: The Science of Climate Change*, edited by J.T. Houghton et al., pp. 407-443, Cambridge Univ. Press, New York, 1996.

Schlesinger, M.E., and N. Ramankutty, Implications for global warming of intercycle solar irradiance variations, *Nature, 360*, 330-333, 1992.

Schlitzer, R., Modeling the nutrient and carbon cycles of the North Atlantic, 2, New production, particle fluxes, CO2 gas exhange, and the role of organic nutrients, *J. Geophys. Res., 94*, 12,781-12,794, 1989.

Shaffer, G., Biogeochemical cycling in the global ocean, 2, New production, Redfield ratios, and remineralization in the organic pump, *J. Geophys. Res., 101*, 3723-3745, 1996.

Shaffer, G. and J.L. Sarmiento, Biogeochemical cycling in the global ocean, 1, A new, analytical model with continuous vertical resolution and high latitude dynamics, *J. Geophys. Res., 100*, 2659-2672, 1995.

Siegenthaler, U., Uptake of excess CO2 by an outcrop-diffusion model of the ocean, *J. Geophys. Res., 88*, 3599-3608, 1983.

Siegenthaler, U., and F. Joos, Use of a simple model for studying oceanic tracer distributions and the global carbon cycle, *Tellus, Ser. B. 44*, 186-207, 1992.

Watts, R.G., Global climate variation due to fluctuations in the rate of deep water formation, *J. Geophys. Res., 90*, 8067-8070, 1985.

Wigley, T.M.L., and S.C.B. Raper, Thermal expansion of sea water associated with global warming, *Nature, 330*, 127-131, 1987.

Wigley, T.M.L., and S.C.B. Raper, Natural variability of the climate system and detection of the greenhouse effect, *Nature, 344*, 324-327, 1990a.

Wigley, T.M.L., and S.C.B. Raper, Future changes in global- mean temperature and thermal-expansion-related sea level rise, in *Climate and Sea Level Change: Observations, Projections and Implications*, edited by R.A. Warrick and T.M.L. Wigley, pp. 111-132, Cambridge Univ. Press, New York, 1990b.

Wigley, T.M.L., A.K. Jain, F. Joos, B. Nyenzi, and P.R. Shukla, *Implications of Proposed CO_2 Emissions Limitations, Tech. Pap. 4*, 41 pp., Intergovernmental Panel on Clim. Change, Geneva, 1997.

Woods, J.D., The physics of thermocline ventilation, in *Coupled Ocean-Atmosphere Models*, edited by J.C.J. Nihoul, pp. 543-590, New York, 1985.

L.D. Danny Harvey, Department of Geography, University of Toronto, 100 St. George Street, Toronto, Ontario, Canada M5S 3G3. (email: harvey@geog.utoronto.ca)

Z. Huang, Atmospheric and Climate Sciences Group, Earth and Environment Sciences Division, EES-8 MS-SD401, Los Alamos National Laboratory, Los Alamos, NM 87545.

(Received April 10, 2000; revised March 13, 2001;
accepted March 20, 2001.)